Finite element simulation of textile materials at mesoscopic scale

Damien Durville

FINITE ELEMENT SIMULATION OF TEXTILE MATERIALS AT MESOSCOPIC SCALE

D. Durville

LMSSMAT, Ecole Centrale Paris / CNRS UMR 8579
Grande Voie des Vignes - F-92295 CHATENAY-MALABRY CEDEX - France
E-mail: damien.durville@ecp.fr

Abstract

This paper presents a finite element simulation of the mechanical behaviour of woven fabrics or textile composites at the mesoscopic scale, i.e. at the scale of contact-friction interactions between elementary fibers. In our model, each fiber constituting the studied woven sample is taken is represented by a finite strain 3D beam, while the focus is put on the detection and taking into account of contact-friction interactions between these beams. The model is first used to compute the unknown initial configuration, by simulating in a sense the weaving process. In a second step, once this initial configuration has been computed, an elastic matrix can be added to the model, in order to simulate and identify the behaviour of the sample under various loading cases.

1. Introduction

The need of characterization of complex and nonlinear mechanical behaviour of textile composites is increasing with their growing use in a wide range of technical applications. The complexity of the macroscopic behaviour of these materials is mainly due to phenomenons occuring at the level of constituting fibers, which can be described as the mesoscopic scale. As long as these local phenomenons remain difficult to investigate experimentally, an in-depth understanding of mechanisms at this mesoscopic scale is still lacking.
The modeling strategies presented here shows that the finite element simulation has become an alternate approach to explore and predict the mechanical behaviour of textile composite materials. To meet such an objective, the simulation has to be able to take into account not only the behaviour of each individual fiber of the structure, but also the interactions developed between fibers. The recent development of computational capacities makes this kind of computations now feasible.
Different approaches to simulate the behaviour of textile structures can be found in the litterature. Some are based on the construction of discrete models, relying on the identification of spring stiffnesses and some geometrical assumptions [1–3]. An other way of doing is to use finite element models, in which individual yarns are represented either by 3D or by beam elements [4, 5]. For this kind of simulation, the identification of transverse behaviour of yarns is a delicate point, with a large influence on the results, which requires a fitting to determine the parameters governing this behaviour. As an alternative, simulations taking into account internal fibers inside yarns have been carried out, using an explicit finite element code, to simulate manufacturing process and mechanical properties of fabrics [6]. In the connected domain of generalized entangled media, we also suggested a modeling approach at the scale of fibers, based on an implicit finite element code [7, 8].
Not stopping at the yarn level, but going down to the fiber level avoids having to specify any model for the behaviour of individual yarns. The only mechanical behaviour that has to be characterized is the one of individual fibers, that can be simply considered as linear elastic.
The purpose of the simulation code we developed, based on an implicit solver, is to consider small samples of textile composites, made of several hundreds of fibers, possibly coated with an elastic layer. The data necessary for the computation, i.e. the description of the global

arrangement of fibers in initially straight yarns, the elastic constants determining the behaviour of fibers and matrix, and the description of the weave type, are easy to collect and to define. Furthermore, most of the tasks, especially the meshing of fibers and matrix, and the detection of different interactions between these parts, are performed automatically by the software. A particularly important point of the method is that the computation of the initial configuration of the woven fabric is handled by the simulation code, by solving a mechanical equilibrium while fulfiling the crossing order between yarns defined by the choosen weaving pattern. This initial stage, bringing comprehensive description of the fabric internal structure, is followed by loading steps, involving an elastic matrix, to simulate various loadings such as biaxial tensile tests, shear tests or bending tests.
In addition to the characterization of the macroscopic behaviour, the simulation at mesoscopic scale offers an accurate description of what occurs in the core of these fibrous materials, both from a geometrical and from a mechanical point of view. This tool can therefore reveal very useful to predict damage and failure caused by various loadings in indiviual fibers. As the modification of any design parameter of the structure is easy to operate, this simulation code is of great interest in order to optimize textile composite materials with respect to various purposes.
In the following, Section 2 is devoted to a general presentation of the approach. The detection and modeling of contact-friction interactions, which are the core of the presented method, are detailed in Section 3. The mechanical coupling between fibers and the matrix, discretized by the means of nonconforming meshes are introduced in Section 4. Finally, Section 5 shows results of the simulation of different loading cases applied to the same initial set of yarns, woven according to two different weave types.

2. Modelling of individual fibers

Special finite strains 3D beam elements have been developped for the present approach. The kinematical model used for these elements is based on a first order expansion of the placement (or displacement) of any material particle of the beam with respect around the line of centroids of the beam. According to this model, the position $\boldsymbol{x}(\xi, t)$ of any material particle ξ, whose coordinates in the reference configuration are denoted (ξ_1, ξ_2, ξ_3) (*Fig. 1*), is assumed to express by the mean of three vector fields as follows

$$\boldsymbol{x}(\xi, t) = \boldsymbol{x}_0(\xi_3, t) + \xi_1 \boldsymbol{g}_1(\xi_3, t) + \xi_2 \boldsymbol{g}_2(\xi_3, t). \tag{1}$$

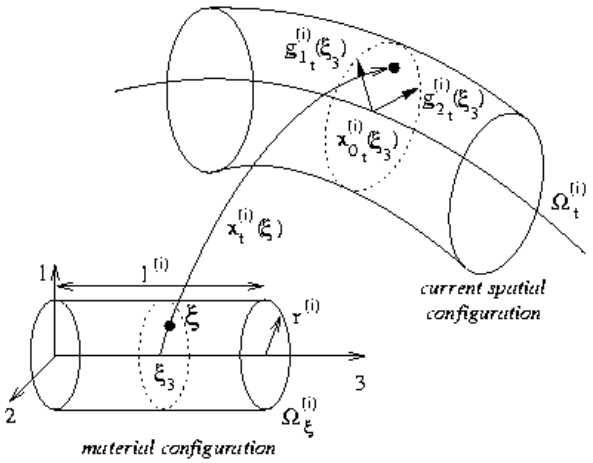

Fig. 1. Description of kinematics

In the above expression, $\boldsymbol{x}_0(\xi_3, t)$ is the position of the centroid of the beam cross-section, while

vectors $\boldsymbol{g}_1(\xi_3, t)$ and $\boldsymbol{g}_2(\xi_3, t)$ can be viewed as two director vectors for the section. The expression of the displacement $\boldsymbol{u}(\boldsymbol{\xi}, t)$ can be derived from the previous expression :

$$\begin{aligned} \boldsymbol{u}(\boldsymbol{\xi}, t) &= \boldsymbol{x}(\boldsymbol{\xi}, t) - \boldsymbol{x}(\boldsymbol{\xi}, 0) && (2) \\ &= \boldsymbol{u}_0(\xi_3, t) + \xi_1 \boldsymbol{h}_1(\xi_3, t) + \xi_2 \boldsymbol{h}_2(\xi_3, t) && (3) \end{aligned}$$

This last expression shows that, according to the assumed kinematical model, the displacement of any material particle of the beam is expressed through three vector fields : a vector $\boldsymbol{u}_0(\xi_3, t)$ standing for the translation of the cross-section's centroids, and the variations of the two sections vectors, $\boldsymbol{h}_1(\xi_3, t)$ and $\boldsymbol{h}_2(\xi_3, t)$. With this model, the kinematics of each cross-section depends on three vector fields and nine degrees of freedom. Since both norms of section vectors and angles between them can vary, the model is able to consider planar deformations of each cross-section, which is an improvement with respect to classical beam models with rigid cross-sections. Moreover this model allows to get rid of the handling of large rotations associated to the assumption of rigid sections.
The Green-Lagrange strain tensor derived from this kinematical model is a full tensor, where no component is a priori zero. This point is important since it enables to use a 3D constitutive law, taking into account all components of the strain tensor. 3D phenomena such as Poisson's effect (contraction of the section coupled with the axial stretching of the beam) can now be captured by the means of this model.

3. Contact detection with an assembly of fibers

3.1. Introduction : use of discrete contact elements

A textile structure appears as an assembly of fibers with contact-friction interactions between themselves. The detection of these interactions between moving fibers is one of the main issue in our approach. The handling of contact is based on the construction of discrete contact elements made of two material particles. For us, a contact element defined at a point $\boldsymbol{x}_c$ is constituted by the two particles that may be predicted to enter into contact at this location. The question that underlies this section are where and how to construct these contact elements within an assembly of fibers.

3.1..1 Limits of classical approaches

Usually, in classic approaches, contact is determined by starting from one point on the surface of a body, whose position is often at a particular location with respect to the finite elements (node or integration point), and searching a candidate to contact on the opposite body, usually in the direction of the normal to one of the surfaces. This method gives good results in many cases, but does not seem adapted for the situations we are interested in. The first reason for this is that, in regions where fibers are strongly curved, the normal direction the the surface of one fiber may point towards a candidate which is actually far from the contact zone that may be predicted. Furthermore, one important disadvantage of this method is that it does not ensure a symmetrical treatment of both surfaces : starting from one surface, and using the normal direction to this surface to determine a candidate on the opposite surface, and then, in a second step, applying again the same process from this candidate, has very little chance to give the same initial point. The main objection that may be raised in relation with these two points, is that using as searching direction the direction normal to only one surface, is, in a sense, like considering only half of the geometry of contact. What is lacking in this way of doing, is to consider simultaneously both surfaces involved in the contact. That is precisely the part we assign to intermediate geometries.

3.1..2 Introduction of intermediate geometries

The part played by the intermediate geometry is to approximate the actual geometry of the contact surface and to provide a geometrical support for the discretization of the contact problem. By this way, the contact problem is set on the intermediate geometry, and the two interacting surfaces are considered symmetrically with respect to this third party.
We define the intermediate geometry, in regions where contact may occur, as the average between the two opposite surfaces that may enter into contact. To do this, such regions have to be delimited by the means of zones of proximity. The way of averaging the two contacting surfaces may be very complex to define in general cases, as it requires the definition of a bijection between these parts of surfaces. In the case of beams, this problem is simplified by the consideration of lines instead of surfaces. The zones of proximity we intend to determine between fibers are simply constituted by parts of their centroidal lines, and the average between the two parts of lines can be defined unambiguously.

3.1..3 Process of determination of contact elements

The goal of this process is to determine pairs of material particles which are predicted to enter into contact, and which constitute contact elements.

Determination of zones of proximity A zone of proximity is defined as two parts of centroidal lines of fibers whose distance to each other is lower than a given proximity criterion. For a proximity criterion δ, the k-th zone of proximity between fibers i and j, denoted $Z_k(i,j)$, may thus be defined as follows (see *Fig. 2*) :

$$Z_k(i,j) = [a^{(i)}, b^{(i)}] \cup [a^{(j)}, b^{(j)}]; \forall (\xi_3^{(i)}, \xi_3^{(j)}) \in [a^{(i)}, b^{(i)}] \times [a^{(j)}, b^{(j)}],$$
$$\|\boldsymbol{x}_{0_t}^{(i)}(\xi_3^{(i)}) - \boldsymbol{x}_{0_t}^{(j)}(\xi_3^{(j)})\| \leq \delta,$$

The determination of these zones of proximity must be fast. For that, for each pair of fibers, the distance is calculated only between some control points coarsely distributed on one fiber, and their corresponding closest points determined on the other fiber. Corrections may be needed in some cases so that the intermediate geometry derived from the zone of proximity has suitable characteristics for a precise detection of contact.

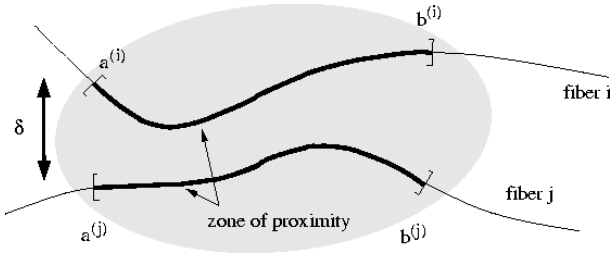

Fig. 2. Determination of zones of proximity

Intermediate geometry For a given zone of proximity, the intermediate geometry is simply defined as the average of the two parts of centroidal lines constituting the zone, on which a relative abscissa s is defined. The same abscissa is used to define each point $\boldsymbol{x}_{int,k}(s)$ of the intermediate geometry in the following way :

$$\forall s \in [0,1],$$
$$\boldsymbol{x}_{int,k}(s) = \frac{1}{2}\left[\boldsymbol{x}_{0_t}^{(i)}\left((1-s)a^{(i)} + sb^{(i)}\right) + \boldsymbol{x}_{0_t}^{(j)}\left((1-s)a^{(j)} + sb^{(j)}\right)\right].$$

The tangent to the intermediate geometry is calculated similarly as the average of tangents to the two centroidal lines.

Discretization of the contact problem by contact elements Considering contact between a pair of fibers, with respect to the intermediate geometry, the question we ask is what particles of both fibers are likely to enter into contact at a given position on this intermediate geometry. The discretization of the contact problem is also regarded with respect to this geometry, by defining some discrete positions where contact elements will be created. The number n_c of contact elements distributed on the zone of proximity $Z_k(i, j)$ depends on the discretization size, and the position $\boldsymbol{c}_l$ of the l-th contact element of the zone is defined as :

$$\boldsymbol{c}_l = \boldsymbol{x}_{int,k}\left(\frac{l}{n_c + 1}\right) \tag{4}$$

The discretization of the contact problem on the intermediate geometry is thus theoretically defined independently on the discretization of fibers. However, to have a good approximation of contact reactions, these different discretization sizes must be kept consistent with respect to each other.

Determination of pairs of beam cross-sections candidate to contact The first step to determine particles of contact elements is to state which cross-sections are likely to enter into contact at the position $\boldsymbol{c}_l$ of a contact element. The curvilinear abscissas $\xi_3^{(i)}$ and $\xi_3^{(j)}$ of these cross-sections are fixed at the intersection between the orthogonal plane to the intermediate geometry at the position $\boldsymbol{c}_l$ of the contact element and the two centroidal lines of fibers, as shown on *Fig. 3*.

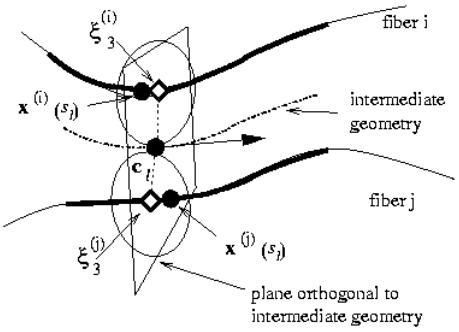

Fig. 3. Determination of cross-sections candidates to contact

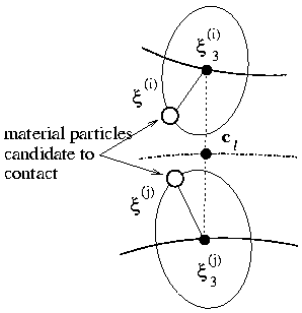

Fig. 4. Determination of material particles contact elements

Determination of materials particles of the contact elements The last step to localize the material particles candidates to contact consists in finding their position on the border of cross-sections. To do this, the direction between the two centroids is projected on each cross-section, and the seeked particles are positioned at the intersections between this projection and the border of the section (*Fig. 4*).
We denote $E_c(\boldsymbol{c}_l)$ the contact element constituted by these two particles determined at the position $\boldsymbol{c}_l$ of the intermediate geometry :

$$E_c(\boldsymbol{c}_l) = \left(\xi^{(i)}, \xi^{(j)}\right) \tag{5}$$

3.1..4 Nonlinear character of the process of determination of contact elements

The process of determination of contact elements is actually a predictive one and depends on the relative positions of fibers, and consequently on the solution itself. For this reason, for each loading step, this process have to be iterated to increase the precision of the determination of particles candidates to contact. Even if the convergence of this iterative process cannot be guaranteed, it shows a good algorithmic behaviour and produce very relevant couples of material particles candidates to contact.

3.2. Mechanical models for contact and friction

3.2..1 Expression of linearized kinematical contact conditions

Normal directions for contact A normal direction has to be set for each contact element to measure the penetration between fibers and to determine the direction of contact reactions. This normal direction may be viewed as the orthogonal direction to a plane acting as a shield between the particles of the contact element, as depicted on *Fig. 5*. The choice of this normal direction is critical, in particular to prevent fibers from going through each other at crossings. To be appropriate to the various relative orientations between fibers that may be encountered, this direction is calculated in function of local geometrical quantities and criteria. In the following, the contact direction for a contact position $\boldsymbol{c}_i$ is denoted $\boldsymbol{N}(\boldsymbol{c}_l)$.

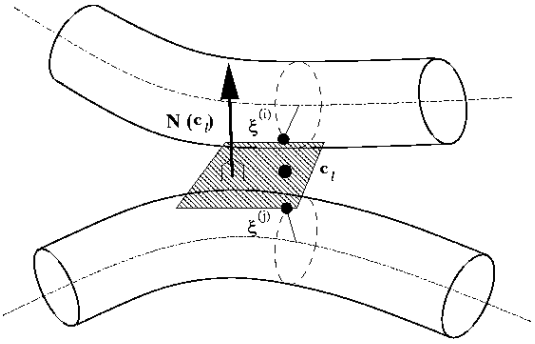

Fig. 5. Definition of the normal direction of a contact element

Expression of the gap for a contact element For a contact element $E_c(\boldsymbol{c}_l) = \left(\boldsymbol{\xi}^{(i)}, \boldsymbol{\xi}^{(j)}\right)$, the gap is calculated as the distance between the two constituting particles, measured along the normal direction $\boldsymbol{N}(\boldsymbol{c}_l)$:

$$gap(\boldsymbol{c}_l) = \left(\boldsymbol{x}_t^{(i)}(\boldsymbol{\xi}^{(i)}) - \boldsymbol{x}_t^{(j)}(\boldsymbol{\xi}^{(j)}), \boldsymbol{N}(\boldsymbol{c}_l)\right) \tag{6}$$

3.2..2 Regularized penalty for contact reactions

Using a classic penalty method, normal reactions are assumed to be proportional to the gap when it is negative. The introduction of a quadratic regularization for very small penetrations stabilizes the contact algorithm by smoothing the contact behaviour. Denoting g_r the penetration threshold characterizing the quadratic part, and k_c the penalty coefficient, the norm of the contact reaction $R_N(\boldsymbol{c}_l)$ is expressed as follows in function of the gap :

$$R_N(\boldsymbol{c}_l) = 0 \text{ if } gap(\boldsymbol{c}_l) \geq 0, \tag{7}$$

$$R_N(\boldsymbol{c}_l) = \frac{k_c}{2}\frac{(gap(\boldsymbol{c}_l))^2}{g_r}, \text{ if } g_r < gap(\boldsymbol{c}_l) < 0, \tag{8}$$

$$R_N(\boldsymbol{c}_l) = k_c\left(gap(\boldsymbol{c}_l) + \frac{g_r}{2}\right), \text{ if } gap(\boldsymbol{c}_l) \leq g_r. \tag{9}$$

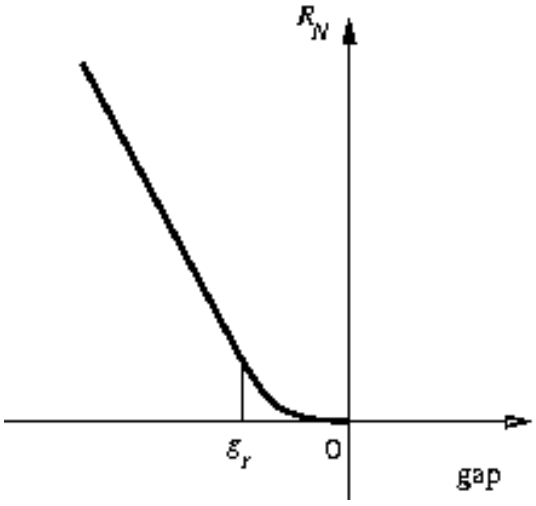

Fig. 6. Representation of the regularized penalty law for contact

3.2..3 Regularized friction law

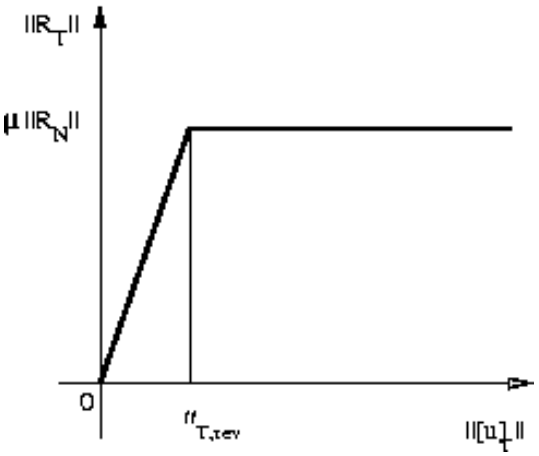

Fig. 7. Representation of the regularized friction model

Denoting $\boldsymbol{u}^{(i)}$ the current displacement field defined on the fiber i, the relative tangential displacement $[\boldsymbol{u}]_T(\boldsymbol{c}_l)$ for a contact element expresses :

$$[\boldsymbol{u}]_T(\boldsymbol{c}_l) = [\boldsymbol{I} - \boldsymbol{N}(\boldsymbol{c}_l) \otimes \boldsymbol{N}(\boldsymbol{c}_l)] \left(\boldsymbol{u}^{(i)}(\boldsymbol{\xi}^{(i)}) - \boldsymbol{u}^{(j)}(\boldsymbol{\xi}^{(j)}) \right). \tag{10}$$

For the tangential reactions, we use a regularized Coulomb's law, which allows a small reversible displacement before pure sliding occurs. The tangential reaction is expressed as follows as function of the tangential relative displacement :

$$\text{if } [\boldsymbol{u}]_T(\boldsymbol{c}_l) \leq u_{T,\text{rev}}, \quad \boldsymbol{R}_T(\boldsymbol{c}_l) = \frac{\mu \|\boldsymbol{R}_N\|}{u_{T,\text{rev}}} [\boldsymbol{u}]_T(\boldsymbol{c}_l) \tag{11}$$

$$\text{else} \quad \boldsymbol{R}_T(\boldsymbol{c}_l) = \frac{\mu \|\boldsymbol{R}_N\|}{\|[\boldsymbol{U}]_T\|} [\boldsymbol{u}]_T(\boldsymbol{c}_l) \tag{12}$$

where μ denotes the Coulomb's friction coefficient, and $u_{T,\text{rev}}$ is the reversible tangential displacement.

3.3. Algorithmic issues

3.3..1 Iterations on nonlinearities

In the presented method, both the process of determination of contact elements, and the normal directions for contact depend on the current position of fibers. Since large increments of displacements are expected, these geometrical entities need to be updated during the computation for each loading step. The convergence of the global algorithm is very sensitive to the order according to which different quantities are updated. To get a good convergence, the algorithm we use for each loading step is made of three embedded loops. The first loop is dedicated to iterations on the determination of contact elements. Then, at a second level, we iterate on the determination of normal directions for contact. Lastly, the inner loop is constituted by iterations of Newton-Raphson type on all other nonlinearities of the problem.

3.3..2 Adjustment of the penalty coefficient for contact

The determination of the two parameters governing the normal contact behaviour, namely the penalty coefficient and the regularization threshold, is a very delicate point of the method. The quadratic regularization of the penalty method shows its best effectiveness from an algorithmic point of view when a significant part of contact elements are concerned by this regularization, that is to say when the gaps of a certain amount of contact elements are lower than the regularization threshold. However, for a given penalty coefficient, the gap of each contact element is function of the force exerted locally between the two interacting fibers. This local force may exhibit both spatial variations, depending on the position in the structure, and time variations related to the evolution of loading. This means that if a unique and constant penalty coefficient is used, penetrations of very different orders may be registered in the structure, which makes the penalty regularization totally ineffective, and prevents the convergence of contact algorithms.
The solution we suggest to face this problem is to control locally the maximum penetration between fibers by adjusting the penalty coefficient. We fix this maximum penetration to a small value proportional to the regularization threshold, this threshold being calculated as a small portion of the typical radius of a fiber. As the construction of contact elements is based on the determination of local zones of proximity, it is easy to assign a particular penalty coefficient for the set of contact elements belonging to the same zone. This local coefficient can therefore be adjusted, each time contact normal directions are updated, in order to control the maximum penetration for each zone.

4. Computation of the initial geometry

One of the interests of the approach presented here is its ability to compute the initial configuration of the woven fabric, only from a description of the arrangement of fibers within each yarn, and a description of the weaving pattern. The geometry of fibers in the initial configuration can not be known a priori since it depends on the rearrangement of fibers and deformations of yarns during the weaving process. The method suggested here to compute this initial configuration can be viewed as a way to simulate the weaving process.
To do this, we start from an arbitrary configuration (*Fig. 8*) where all yarns are straight, lying on the same plane and interpenetrating each other. The task of this initial computation is to make all yarns respect the superimposing order prescribed by the weaving pattern at each crossing between yarns. This pattern states which yarn must be above or bellow the other yarns at each crossing. During steps needed for this stage (around five steps), the same superimposing order is presribed to contact contact conditions between fibers belonging to different yarns : for such fibers in contact, the normal contact direction is taken parallel to the vertical direction, and the sign of the calculated gap is chosen depending on the crossing order between yarns. By

this way, fibers of different yarns, initially penetrating each other, go progressively above each other, until fibers from different yarns are really separated. At the end of this process, ordinary contact conditions can be considered between all fibers. The obtained configuration (*Fig. 9*) is thus computed as the solution of a mechanical equilibrium while fulfiling contact conditions within and between yarns.

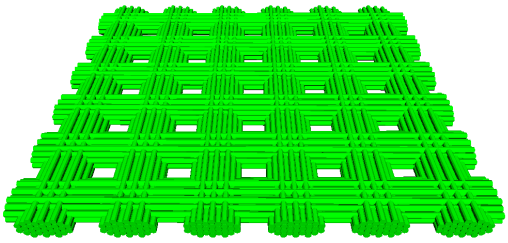

Fig. 8. Starting configuration

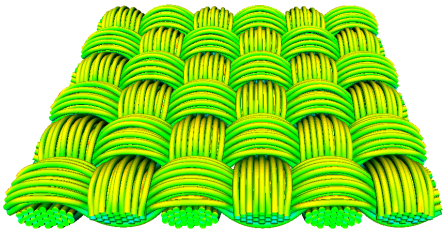

Fig. 9. Computed initial configuration

During this computation of the initial geometry, one end of each yarn is clamped on one side, while the other end is free to move horizontally and is only submitted to a small axial force to maintain a tension. By this way weft and warp yarns are free to shrink, as shown on *Fig. 10*.

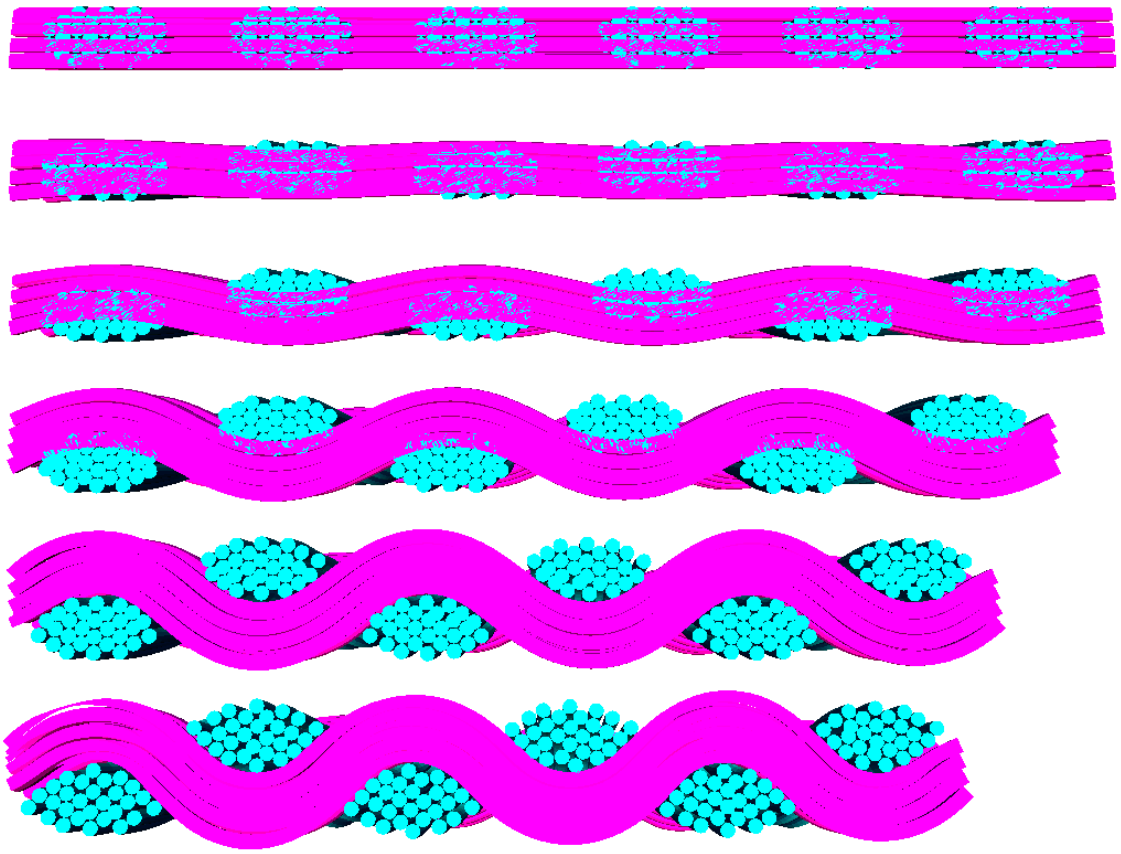

Fig. 10. Cuts of configurations at different steps during the process of computation of the initial configuration

Many useful informations can be derived from this computation of the initial configuration. At the scale of yarns, shrinkages in both weft and warp directions are provided as results of this simulation. Various geometrical quantities, such as the shape of cross-sections along yarns, or the local curvatures for all fibers, are also available as results.

5. Adding of an elastic matrix

In order to consider textile composite samples, it is necessary to add the computed woven structure an elastic matrix. Because of the small size of the fibers, meshing the matrix with a mesh exactly conforming with the geometry of fibers would lead to complex geometrical operations and to expensive computational costs. To overcome these difficulties, the volume of the matrix is meshed coarsely, in such a way it overlaps slightly the outer fibers of yarns (*Fig. 11*).

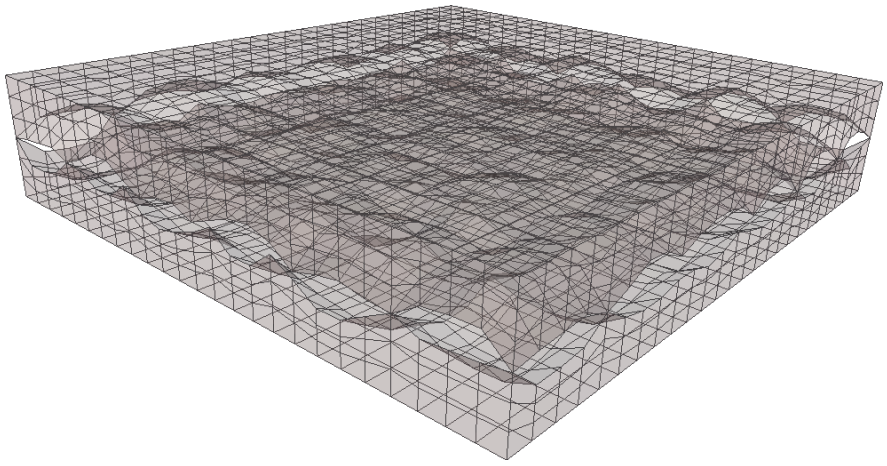

Fig. 11. Mesh of the elastic matrix added to the woven fabric

Doing this way, meshes of the matrix and of the fibers are totally non-conforming, and do not share any node. To ensure a mechanical coupling between the two structures, junction elements are automatically constructed in the overlapping area between fibers and matrix. These junctions elements couple pairs of material particles – one belonging to a fiber, and the other belonging to the matrix. The difference between the displacements of the two particles is penalized with a coefficient equal to the Young's modulus of the matrix.

6. Driving of boundary conditions through rigid bodies

The driving of boundary conditions of the borders of the studied sample is an important issue. Rigid bodies have been introduced in the model to allow a versatile driving of these conditions. At a first level, a rigid body is created at each end of a yarn. The role of these rigid bodies is to gather all ends of fibers of the same yarn. Boundary conditions at the end of fibers are prescribed with respect to these rigid bodies. Then, at a second level, a rigid body is created for each side of the sample. All rigid bodies attached to the yarns on this side, and all nodes on the border of the matrix on this side are linked the rigid body constructed on this yarn. Each of these rigid bodies can be driven either by displacement/rotation, or by force/moment, which offers a wide range of combinations for possible boundary conditions.

7. Numerical results

7.1. Presentation of the sample

The same sample has been used for all results presented here. The woven sample is made of 12 yarns (*Fig. 8*), has each of them being constituted of 28 fibers. Representative figures of this model are summarized in Tab. *1*. The high number of degrees of freedom ($\approx$ 335 000) makes the model a good example of what can be handled by this kind of simulation.

Number of yarns	12
Number of fibers	336
Number of fiber nodes	≈ 37 000
Number of dofs for fibers	≈ 335 000
Number of matrix nodes	≈ 5 400
Number of dofs for the matrix	≈ 16 000
Total number of dofs	≈ 352 000
Number of contact elements	≈ 75 000

Table 1. Description of the model

7.2. **Shear test**

The shear test was simulated without coating in order to capture nonlinear phenomena due to the locking between yarns as the shear angle increases. To perform this test, one side of the sample isq clamped, while an incremental displacement is prescribed on the oppposite side, in a direction parallel to this side. Displacements in directions orthogonal to this side are left free. The two other lateral sides are also left free. The final configuration, after shearing, is shown on *12*.

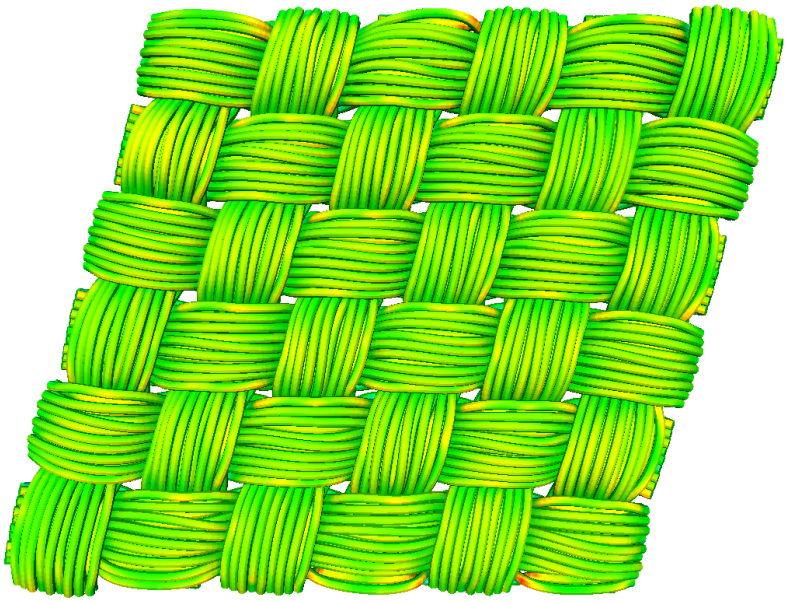

Fig. 12. Deformed mesh of the woven sample after shearing

The shear force (*Fig. 13*) shows a characteristic nonlinear effect due to the locking between yarns.

7.3. **Bending test**

To simulate a bending test, opposite rotations are applied to the rigid bodies attached to two opposite sides of the sample, while horizontal displacements are left free for one of these rigid bodies. The view of the deformed mesh after bending is shown on *Fig. 14*. On the cut of the final configuration (*Fig.* **??**), voids appearing on the side of the composite which is under compression can be observed. This example shows the ability of the simulation to capture interesting local phenomena.

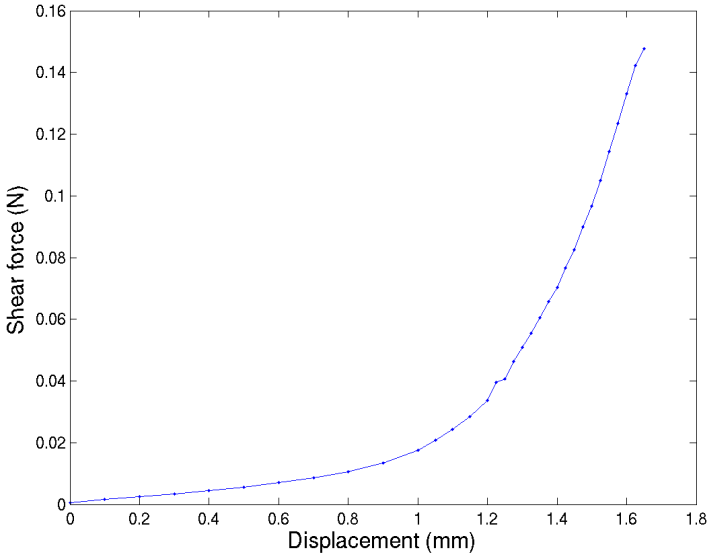

Fig. 13. Loading curve for the shear test

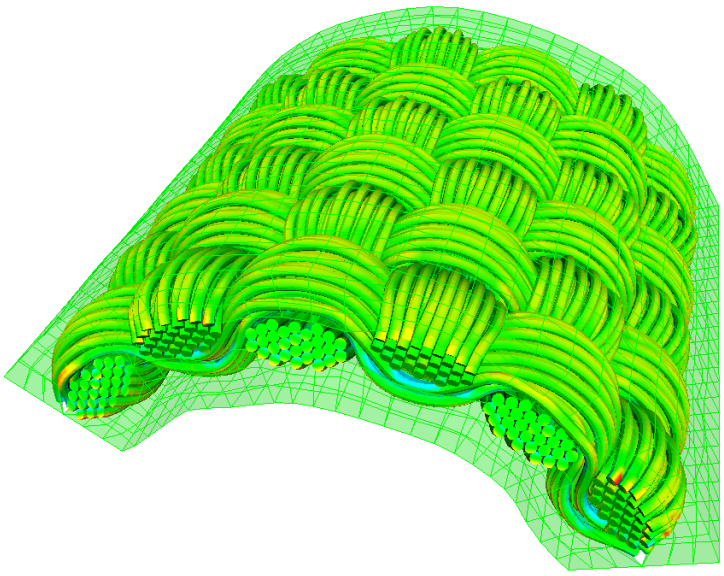

Fig. 14. Deformed mesh of the textile composite sample after bending

7.4. Twisting test

For the twisting test, two opposite rotations are applied to two opposite sides of the sample, around the directions normal to these sides. The view of the final configuration (*Fig. 16*) shows another example of a loading inducing large displacments.

7.5. CPU costs

The computations for the presented tests have been run on a cluster, using 6 processors. The simulation of each step requires about 30 to 40 global iterations, leading to an average of 2 hours CPU time per step for the sample of woven fabric without coating, and 3 hours for the textile composite sample. The simulation of the shear test, with 30 loading steps took around 60 hours,

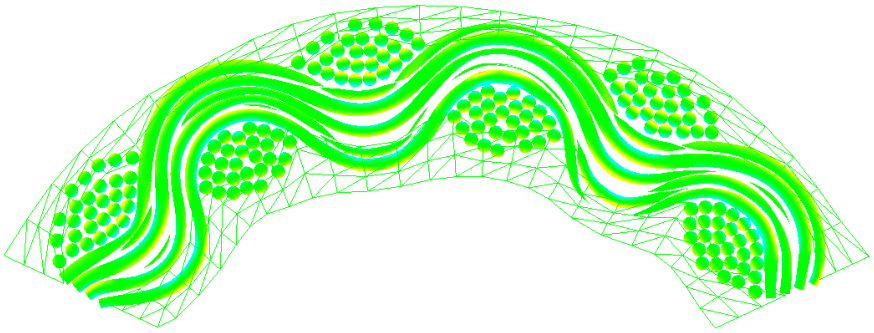

Fig. 15. Cut of the final configuration of the sample submitted to bending

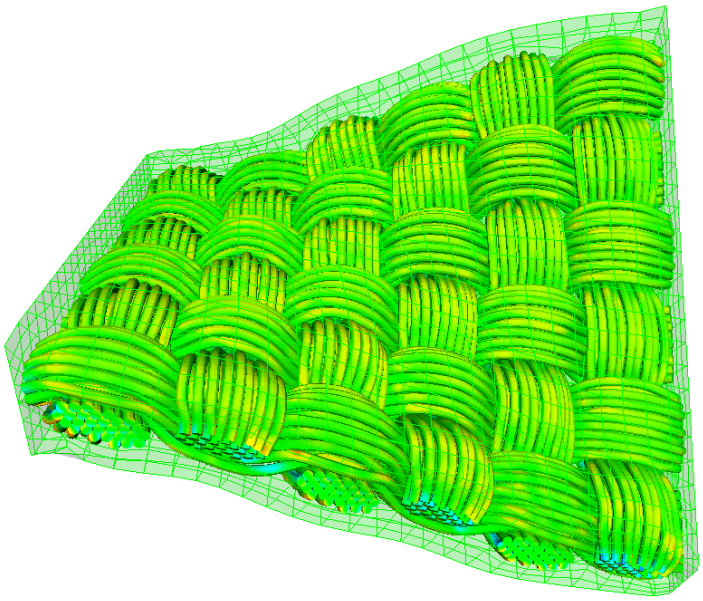

Fig. 16. Deformed mesh of the textile composite sample submitted to a twistng test

while simulations of the bending and twisting tests, carried out with 15 increments, took about 45 hours.

8. Conclusion

The models and algorithms developed to take into account contact-friction interactions taking place within assemblies of fibers undergoing large deformations find an application with the simulation of woven fabric and textile composite samples. The results presented above show that the suggested methodology makes the finite element simulation available to study the mechanical behaviour of textile structures at the scale of interactions between individual fibers.
Thanks to this method, the behaviour of textile structures
The results show that, thanks to the development of accurate, robust and effective methods to take into account contact-friction interactions between fibers, numerical simulation appears nowadays as a possible means to explore the mechanical behaviour of textile composites at the scale of fibers.
The comprehensive approach we suggest lies on the one hand on original geometrical processes, based on the construction of intermediate geometries in contact zones, to detect and discretize contact interactions, and on the other hand on adapted mechanical models associated with fine-tuned algorithms to solve global problems involving numerous nonlinearities. Using an implicit

solver, the developed software allows the simulation of complex structures, characterized by high numbers of degrees of freedom and of contact elements, with a reasonable CPU time.
The main interest of this kind of simulation at mesoscopic scale, beyond the identification of macroscopic behaviour of textile composites, is to provide an in-depth description of phenomenons occuring at this scale, which would remain otherwise out of reach of experiment. The estimation of curvatures, strains and stresses at the level of individual fibers is a major benefit of the approach to study local phenomenons such as damage. This approach should therefore be helpful to optimize the structure of textile composite materials with respect to both global and local criteria.

References

1. N. Bridgens, P. Gosling, M. Birchall, Membrane material behaviour: concepts, practice and develoments, The Structural Engineer 82 (14) (2004) 28–33.

2. B. H. B. Ben Boubaker, J.-F. Ganghoffer, Mesoscopic fabric models using a discrete mass-spring approach: Yarn-yarn interactions analysis, Journal of Materials Science 40 (22) (2005) 5925 – 5932.

3. D. Ballhause, M. König, B. Kröplin, A microstructure model for fabric-reinforced membranes based on discrete element modelling, in: E. O. nate, B. Kröplin (Eds.), Textile Composites and Inflatable Structures II, Structural Membranes 2005, ©CIMNE, Barcelona, Stuttgart, Germany, 2005, pp. 255–263.

4. P. Boisse, B. Zouari, A. Gasser, A mesoscopic approach for the simulation of woven fibre composite forming, Composites Science and Technology 65 (3-4) (2005) 429–436.

5. D. Durville, Modélisation par éléments finis du comportement mécanique de structures textiles : de la fibre au tissu, Revue Europénne des Éléments Finis 11 (2-3-4) (2002) 463–477.

6. H. Finckh, Numerical simulation of mechanical properties of fabrics - weaving / numerische simulation der mechanischen eigenschaften textiler flächengebilde - gewebeherstellung, Proceedings of the German 3rd LS-DYNA Forum 2004, Bamberg, Germany, 2004.

7. D. Durville, Numerical simulation of entangled materials mechanical properties, Journal of Materials Science 40 (22) (2005) 5941–5948.

8. D. Durville, Recent Advances in Textile Membranes and Inflatable Structures, Springer Verlag, 2007, Ch. Finite element simulation of the mechanical behaviour of textile composites at the mesoscopic scale of individual fibers.